# Numerical Investigation of Thermal and Chemical Nonequilibrium Flows past Slender Blunted Cones

Sergey V. Zhluktov*
*Institute for Computer-Aided Design, Moscow 123056, Russia*
and
Sergey V. Utyuzhnikov† and Grigoriy A. Tirskiy‡
*Moscow Institute of Physics and Technology,
Moscow 141700, Russia*

A steady laminar axisymmetric flow of viscous, heat conducting, nonequilibrium, partially dissociated, and ionized air past a thin slender sphere-cone is considered. The flowfield characteristics with the interplay between reactions and vibrational relaxation taken into account are investigated. An "adiabatic" dissociation model accounting for both nonequilibrium excitation of vibrational modes and equilibrium excitation of rotational modes of the air molecules is used to calculate thermal nonequilibrium dissociation rate constants. In the case of thermal equilibrium, the model yields a good agreement of dissociation constants with experimental data widely used in hypersonic calculations. The combined effect of the multicomponent diffusion with real binary diffusion coefficients on the heat transfer rates has been evaluated. Quantitative assessments of the influence of thermal nonequilibrium on the flow parameters have been obtained at various freestream conditions. The influence of the body surface activity with respect to accommodation of vibrational energy on the heat transfer rate has been evaluated.

## I. Introduction

**P**HYSICAL–CHEMICAL processes in the shock layer formed by a highly supersonic airflow past a slender spherically blunted body are simulated. A steady laminar axisymmetric flow of viscous, heat conducting, nonequilibrium, and partially dissociated and ionized air is considered throughout the whole domain between the body surface and the shock wave.

The viscous shock layer (VSL) model[1,2] is used for the simulation. The model results from the full Navier–Stokes equations by neglecting terms less than $Re^{-1/2}$. It is well known[3] that VSL equations yield better accuracy in the downstream region, where the shock-layer thickness is not smaller than Cheng's model of a thin viscous shock layer (TVSL).[4] Furthermore, the VSL model provides better results for the flowfield than the asymptotic theory of a high-order boundary layer at moderate Reynolds numbers.

The effect of chemical and thermal nonequilibrium on the flow characteristics with mutual influence of chemical reactions and vibrational relaxation taken into account is investigated along the body. This problem was studied in detail[5] for the flow around a spherical body. However, the coupling vibration dissociation vibration (CVDV) model used in those researches contains an indefiniteness because the probability of molecular dissociation from different vibrational levels in that model is an exponential function with one empirical (unknown in general) parameter determined by the postulated dissociation activity of upper vibrational levels (preferential

removal model[6]). The fundamental results obtained in Ref. 5 revealed the influence of this indefiniteness on the heat transfer rates to the body and on the other hydrodynamic parameters in the shock layer near the stagnation point. An approach based on the quantum consideration of the dissociation process has been suggested[7] in order to develop a dissociation model without this indefiniteness. An adiabatic model[7] takes into account both the nonequilibrium excitation of vibrational modes (the vibrational temperature does not equal the translational one) and the equilibrium excitation of rotational modes of the molecules (rotational temperature equals translational one). The cross sections and potentials of intermolecular interaction introduce the only uncertainty into the model due to the scatter in the corresponding published data. Formulas to approximate the adiabatic model have been subsequently suggested.[8] The formulas are simple enough to be applied to complicated gasdynamic calculations. In that paper[8] the adiabatic model was used for numerical investigation of the flow in a chemical and thermal nonequilibrium viscous shock layer over a spherical body. The comparisons of adiabatic dissociation constants with experimental data under thermal equilibrium have shown that the model agrees well with data of Blottner and Part at $T \leq 10,000$ K and with the data of Baulch (for $O_2$) and Kewley (for $N_2$) at $T \geq 10,000$ K (Ref. 8) (see Sec. III).

The model of Ref. 7 approximated by the formulas of Ref. 8 is used in this article to study chemical and thermal nonequilibrium flows of viscous heat conducting air past a slender spherically blunted cone. The block-marching method of global iterations[9–12] is used to integrate the axisymmetric VSL equations along the body.

## II. Governing Equations

Let us consider a hypersonic flow of a viscous heat conducting chemically reacting air past a slender spherically blunted cone at freestream velocities $V_\infty \leq 8$ km/s and Reynolds numbers $Re_\infty \geq 1000$. The nine-species ionized air ($O_2$, $N_2$, NO, O, N, $NO^+$, $N_2^+$, $N^+$, E—electron) is considered. The trans-

lational and rotational modes of the particles are assumed to be in equilibrium at the translational temperature $T$. But there is no equilibrium between active (translational, rotational) and vibrational modes. The vibrational quantum states of the $i$th molecular species are assumed to be populated according to a Boltzmann distribution at a vibrational temperature $T_i^{(v)}$. (In general, $T_i^{(v)} \neq T$.) The contribution from the excited electronic quantum states of the species into the total internal energy of the mixture is neglected. It is assumed that all the heavy particles are in the ground electronic state from which ionization takes place. Radiation, barodiffusion, and thermodiffusion are not taken into account. Barodiffusion has a greater effect on the flow characteristics than thermodiffusion because the barodiffusion coefficients are greater than the thermodiffusion ones by an order of magnitude. The species concentrations are redistributed and the diffusion fluxes are changed due to the barodiffusion in a neighborhood of the shock wave,[13] where the gradients of the pressure and other hydrodynamic characteristics are maximum. At the same time, barodiffusion has practically no influence on the velocity, pressure, density, and temperature within the shock layer. The heat transfer rate onto the body surface is at most 2% less and the temperature of the radiatively equilibrium surface is at most 10 deg less than corresponding values calculated without barodiffusion taken into account. The influence of chemical reactions occurring in the shock wave on the heat transfer rate to the body surface is small (no more than 1%)[13] and can be neglected. Therefore, the problem of the flow in the shock wave can be separated from that in the viscous shock layer (two-layer model of Cheng[4]). Radiation does not change the structure of the shock-layer flow substantially at freestream conditions discussed and can also be neglected.[14]

Consider the most important from the two-dimensional (axisymmetric) VSL equations. The system is written in an orthogonal coordinate system $(x, y)$ normally connected to the body surface, $x$ being measured from the stagnation point along the surface and $y$ being measured along the normal direction from the surface to a given point. In these coordinates the normal projection of the momentum conservation equation has the following form:

$$\rho \left( \frac{v_1}{H_1} \frac{\partial v_2}{\partial x} + v_2 \frac{\partial v_2}{\partial y} - \frac{v_1^2}{RH_1} \right) = -\frac{\partial P}{\partial y} \tag{1}$$

where $\rho$ is the mass density, $v_1$ and $v_2$ are the tangential and normal components of the velocity, respectively, $H_1 = 1 + y/R$ and $r = r_w + y \cdot \cos \alpha$ are the metric coefficients, $R(x)$ is the radius of the surface curvature, $r(x, y)$ is the distance from a given point to the axis of symmetry, $r_w(x)$ is the distance from the body surface to the axis of symmetry, $\alpha$ is the angle between a tangent to the body surface and the axis of symmetry, and $P$ is the static pressure of the mixture. The normal component of the energy flux can be written via the full mixture enthalpy:

$$J_{Hy} = -\frac{\lambda}{C_p} \left( \frac{\partial H}{\partial y} - v_1 \cdot \frac{\partial v_1}{\partial y} - v_2 \cdot \frac{\partial v_2}{\partial y} - \sum_{i=1}^{N} h_i \frac{\partial c_i}{\partial y} \right)$$
$$- v_1 \tau_{xy} + \sum_{i=1}^{N} h_i J_{iy} \tag{2}$$

$\lambda$ is the thermal conductivity, $C_p$ is the specific heat of the mixture at a constant pressure, $h_i$ is the static enthalpy of species $i$, $N$ is the total number of species, $\tau_{xy}$ is the viscous shear stress, $J_{iy} = \rho c_i(v_{2i} - v_2)$ is the normal component of the diffusion flux of species $i$, $c_i$ is the mass fraction of the species, and $v_{2i}$ is the normal component of the $i$th species average velocity. For $c_i$ the species mass conservation equations are used. The equations are closed by Stefan–Maxwell's

relationships. Baro- and thermodiffusion neglected, these relationships for quasineutral gas mixture are given by[3]

$$\frac{\partial c_i}{\partial y} = -J_{iy} \frac{S_i}{\mu} - \frac{c_i}{\mu} \sum_{j=1}^{N} J_{jy} \left\{ -\frac{m}{m_j} S_{ij} + \sum_{k=1}^{N} S_{jk} c_k \left( \frac{m}{m_j} - \frac{m}{m_k} \right) \right.$$
$$\left. - \frac{e_i - \sum_{k=1}^{N} c_k e_k}{\sum_{k=1}^{N} c_k \frac{e_k^2}{m_k}} \frac{1}{m_j} \left[ e_i S_i - m \sum_{k=1}^{N} S_{jk} e_k \frac{c_k}{m_k} \right] \right\} \tag{3}$$

where $e_i$ is the electric charge of species $i$, $\mu$ is the viscosity

$$S_i = \sum_{j=1}^{N} S_{ij} x_j$$

$S_{ij}$ is the binary Schmidt's number for the $i$-$j$th colliding pair, $x_j$ is the molar fraction of species $j$

$$m = \sum_{j=1}^{N} m_j x_j$$

is the average molar mass of the mixture, and $m_j$ is the molar mass of species $j$. It is assumed that the quasineutrality condition

$$\sum_{j=1}^{N} x_j e_j = 0 \tag{4}$$

holds for the mixture and the electric current equals zero throughout the layer:

$$\sum_{j=1}^{N} \frac{e_j}{m_j} J_j = 0 \tag{5}$$

Let us introduce the mass fractions ($c_j^*$) and diffusion fluxes ($J_j^*$) of the elements:

$$c_j^* = c_j + \sum_{k=L+1}^{N} \nu_{kj} \frac{m_j}{m_k} c_k, \quad J_j^* = J_j + \sum_{k=L+1}^{N} \nu_{kj} \frac{m_j}{m_k} J_k$$
$$j = 1, 2, \ldots, L$$

Here it is assumed that the first $L$ species are elements (in the present study these are $O_2$, $N_2$, and E), $\nu_{kj}$ are stoichiometric coefficients. It is easy to show that conditions (4) and (5) are equivalent to the conditions of zero $c_E^*$ and $J_E^*$:

$$c_E^* = \frac{m_E}{m} \sum_{j=1}^{N} x_j e_j = 0, \quad J_E^* = m_E \sum_{j=1}^{N} \frac{e_j}{m_j} J_j = 0$$

Therefore, the molar fraction and the diffusion flux of electrons can be calculated from relationships (4) and (5) rather than by solving the mass conservation equation for electrons. The other $L$-1 species mass conservation equations for elements, being formulated in terms of $c_E^*$ and $J_E^*$, have no source terms [their right-hand sides (RHSs) equal zero]. Practically, only $L$-2 from these equations are solved because of the evident relationships:

$$\sum_{j=1}^{N} c_j = \sum_{j=1}^{L} c_j^* = 1, \quad \sum_{j=1}^{N} J_j = \sum_{j=1}^{L} J_j^* = 0 \tag{6}$$

The number of mass conservation equations with nonzero source terms is $N - L$ and corresponds to the number of species produced in chemical reactions. Besides, the Stefan–

Maxwell relationships must be rearranged so that the quantities $c_j^*$ and $J_j^*$ enter explicitly both the left-hand side (LHS) and RHS. The VSL equation set is closed by the equation of state and an evident relationship between the total (dynamic) enthalpy $H$ and the static enthalpies of species $h_i$, which the relationship uses to determine the temperature of active modes of the mixture particles after the energy conservation equation has been solved.

Equations (1–6) together with (omitted here) species mass conservation equations, tangential projection of the momentum conservation equation, and the energy conservation equation (see Ref. 3) is called the multicomponent nonequilibrium viscous shock layer (MN VSL) equation set for simulating the flow past a planar (axisymmetric) blunt body. In the case of thermal nonequilibrium, when there is no equilibrium between different modes, relationships describing energy exchange between different quantum states of species must be included into the MN VSL system. When the translational and rotational modes are in equilibrium, the vibrational quantum states of the molecular species $i$ are populated according to the Boltzmann distribution at a vibrational temperature $T_i^{(v)} \neq T$, and all the particles are in the ground electronic state, then the $i$th vibrational energy conservation equation (equation of vibrational relaxation) can be written in terms of the macroscopic average vibrational energy of the $i$th molecular species, and all such equations must be solved together with the previously discussed equations. According to Ref. 15, the equation of vibrational relaxation for a molecular species $i$ can be written as follows:

$$\rho \left[ \frac{v_1}{H_1} \frac{\partial}{\partial x}(\varepsilon_i c_i) + v_2 \frac{\partial}{\partial y}(\varepsilon_i c_i) \right]$$
$$+ \frac{1}{H_1 r^\nu} \frac{\partial}{\partial y}\left[ H_1 r^\nu \left( \varepsilon_i J_{iy} - \mu \frac{c_i}{S_i} \frac{\partial \varepsilon_i}{\partial y} \right) \right] = W_i^{(v)} \quad (7)$$

where $\varepsilon_i[T_i^{(v)}]$ is the average vibrational energy of the $i$th species, $\nu = 0$ for a planar flow and $\nu = 1$ for an axisymmetric flow. In order to calculate this quantity, the model of harmonic oscillator cutoff at the dissociation energy $D = kT_{Di}$ ($k$ is the Boltzmann constant and $T_{Di}$ is the dissociation characteristic temperature of the species $i$) is used in this article:

$$\varepsilon_i = R_A \left\{ \frac{\theta_i}{\exp[\theta_i/T_i^{(v)}] - 1} - \frac{T_{Di}}{\exp[T_{Di}/T_i^{(v)}] - 1} \right\} \quad (8)$$

here, $\theta_i$ is the vibrational characteristic temperature of the $i$th species and $W_i^{(v)}$ is the vibrational source term accounting for the energy exchange between vibrational quantum states of the $i$th molecular species and other modes of the particles. In general, $W_i^{(v)}$ includes the rates of the energy exchange between the vibrational modes of the $i$th molecules and the active modes of heavy particles ($V$-$T$ exchange), vibrational modes of the other molecular species ($V$-$V'$ exchange), and free electrons ($E$-$V$ exchange), along with the loss (gain) of vibrational energy in dissociation (recombination). It is well known that characteristic vibrational temperatures of the air molecules differ at most by 50%. The $V$-$V'$ exchange is much faster than the $V$-$T$ exchange. Hence, it can be assumed that all the molecular species of the mixture have a Boltzmann distribution with the same average vibrational temperature $T_i^{(v)} = T^{(v)}$ and the term due to the $V$-$V'$ process can be neglected. Therefore, a two-temperature thermodynamic model is considered. The $E$-$V$ term is also neglected because it is small under the condition of low ionization (when $V_\infty \leq 8$ km/s). Therefore, $W_i^{(v)}$ is the sum of two terms:

$$W_i^{(v)} = c_i \frac{\varepsilon_i(T) - \varepsilon_i[T^{(v)}]}{\tau_i} - W_{Di} \quad (9)$$

Realistic values of the vibrational relaxation time $\tau_i$ (Ref. 16) at high temperatures ($T \geq 10^4$ K) are calculated in this article by using the Park correction procedure for $\tau_i$ (Ref. 17)

$$\tau_i = \left\{ P_{atm} \sum_r x_r \exp[18.42 - 1.16 \times 10^{-3} \mu_{ir}^{1/2} \theta_i^{4/3}(T^{-1/3}$$
$$- 0.015\mu_{ir}^{1/4})] \right\}^{-1} + \{\sigma_v \langle V_i \rangle n\}^{-1}, \quad \mu_{ir} = \frac{m_i m_r}{m_i + m_r} \quad (10)$$

where $P_{atm}$ is the pressure measured in atmospheres, $\langle V_i \rangle$ is the average heat speed of the molecular species $i$, and $n$ is the concentration of the mixture particles. Millikan and White's term is summed only over heavy particles. According to Ref. 18, $\sigma_v$ is given by

$$\sigma_v = 10^{-17}(50,000/T)^2 \text{ cm}^2 \quad (11)$$

The source term $W_{Di}$ (Ref. 3) accounts for the influence of chemical reactions on vibrational relaxation:

$$W_{Di} = \rho^2 m_i \left\{ K_{Di}[T, T^{(v)}] \frac{c_i}{m_i} \varepsilon_i(T_m) \right.$$
$$\left. - \rho K_{Ri}(T) \frac{c_{A1}}{m_{A1}} \frac{c_{A2}}{m_{A2}} \frac{R_A T_{Di}}{2} \right\} \quad (12)$$

$$T_m^{-1} = [T^{(v)}]^{-1} - T^{-1} \quad (13)$$

where $A_1$ and $A_2$ are the atoms of the molecular species $i$, $K_{Di}$ is the dissociation rate constant, $K_{Ri}$ is the recombination rate constant, $\varepsilon_i(T_m)$ is the average value of vibrational energy lost by the vibrational modes in a single dissociation, and $R_A T_{Di}/2$ is the average energy gained in a single recombination. Summing Eq. (7) over the molecular species, one can obtain the equation for $T^{(v)}$.

It should be emphasized that in the case of thermal nonequilibrium, expression (2) must be transformed so that the term due to the flux of vibrational energy (the last term in the following equation) enters it explicitly[15]:

$$J_{Hy} = -\frac{\lambda^{act}}{C_p^{act}} \left( \frac{\partial H}{\partial y} - v_1 \cdot \frac{\partial v_1}{\partial y} - v_2 \cdot \frac{\partial v_2}{\partial y} - \sum_{i=1}^N h_i \frac{\partial c_i}{\partial y} \right) - v_1 \tau_{xy}$$
$$+ \sum_{i=1}^N h_i J_{iy} - \frac{\partial T^{(v)}}{\partial y} \frac{\lambda^{act}}{C_p^{act}} \sum_{j=M} \varepsilon_j' \frac{c_j}{m_j} \left( \frac{Pr^{act}}{S_j} - 1 \right) \quad (14)$$

where a prime designates a derivative with respect to the vibrational temperature $T^{(v)}$; $\lambda^{act}$, $C_p^{act}$, and $Pr^{act}$ are the heat conductivity, the specific heat of the mixture per unit mass at a constant pressure, and the Prandtl number due to the active modes, respectively; "$j = M$" means summing over molecular species:

$$h_A = h_A^0 + 2.5 \cdot R_A T/m_A \quad (15)$$

$$h_M = h_M^0 + \{3.5 \cdot R_A T + \varepsilon_M[T^{(v)}]\}/m_M \quad (16)$$

$h_A^0$ and $h_M^0$ are the heats of formation of atoms and molecules, respectively.

## III. Model of Intermolecular Processes

The adiabatic dissociation model[7] is used in this article to simulate vibrational nonequilibrium dissociation. The main ideas of Ref. 7 are briefly outlined next.

For gases consisting of weakly interacting particles we can assume that each energy level can be split into independent modes, describing the translational motion of the mass center

of the molecule, rotational motion of the molecule, and vibrational motion of the molecular atoms, respectively. We will assume that the molecule under consideration is at the ground electronic state. Therefore, the potential energy of the molecule at the $(v, J)$th vibrational–rotational quantum state $(J \gg 1)$ can be expressed as follows:

$$E_{vJ} = E_v + E_J, \quad E_v = kv\theta(1 - \xi v), \quad E_J = BJ^2 \quad (17)$$

Here, $\xi = k\theta/4D$ ($\xi = 0$ when the molecule is considered as a rigid rotator–harmonic oscillator) and $B$ is the rotational constant. Assume that the cross section of dissociation from the $(v, J)$th vibrational–rotational level depends only on the number of vibrational level $v$ and do not depend on the rotational quantum number $J$:

$$\sigma_{vJ} = \sigma_v = \sigma_0 \exp\{-[(D - E_v)/h\alpha_0 u]\} \quad (18)$$

here, $\sigma_0$ is an effective cross section of molecular disintegration from the states near dissociation limit, which is close to the gas-kinetic cross section; $h$ is Planck's constant; $\alpha_0$ is the parameter of repulsive interaction potential

$$V = V_0 \exp(-\alpha_0 r) \quad (19)$$

$r$ (Å) is the distance between interacting particles; and $u$ is a relative velocity of colliding particles. The use of adiabatic principle (18) accounts for molecular disintegration from all the vibrational levels, including ground vibrational state without the introduction of any effective level. The principle enables one to describe dissociation at high temperatures $(T \geq D/2k)$. For the constant of dissociation from the $(v, J)$th level in a general case we have

$$k_{vJ} = \int_{E_{vJ}}^{\infty} \sigma_{vJ} u f(u)\, du \quad (20)$$

where $f(u)$ is Maxwellian distribution. Assume that $\sigma_{vJ} = 0$ at $u < u_b$ and $\sigma_{vJ} = \sigma_v = \mathrm{const}(u_b)$ at $u > u_b$, where $u_b$ is determined by the expression:

$$\tfrac{1}{2}\mu u_b^2 = N_A(D - E_v) \quad (21)$$

here, $\mu$ is the reduced mass of colliding particles and $N_A$ is the Avogadro number. Then the integration of Eq. (20) yields

$$k_{vJ} = \sigma_v \left(\frac{8R_A T}{\pi\mu}\right)^{1/2} \left(\frac{D - E_v}{kT} + 1\right) \exp\left(-\frac{D - E_v}{kT}\right) \quad (22)$$

It is obvious that

$$K_D = \sum_{v=0}^{v_{max}} \sum_{J=0}^{J_{max}} k_{vJ} f_{vJ} \quad (23)$$

In the case of a Boltzmann distribution over rotational levels with translational temperature $T$ and over vibrational levels with vibrational temperature $T^{(v)} \neq T$, we have for distribution function $f_{vJ}$

$$f_{vJ} = \frac{1}{Z_{vib} Z_{rot}} \exp\left[\frac{-E_v}{kT^{(v)}}\right] 2J \exp\left(\frac{-E_J}{kT}\right) \quad (24)$$

where $Z_{rot} = T/B$ is the rotational partition function and $Z_{vib}[T^{(v)}]$ is the vibrational partition function taken as that of harmonic oscillator cutoff at the energy of dissociation. $v_{max}$ in Eq. (23) is the maximum vibrational level corresponding to the border of continuous spectrum. The maximum value of rotational quantum number $J_{max}$ for the $v$th vibrational

level is determined from the condition of rotational dissociation of the molecule from the level

$$BJ_{max}^2 = D - E_v \quad (25)$$

We neglect here potential threshold due to rotational excitation of molecules. Integrating Eq. (23) instead of summing up over rotational levels, we obtain the following expression for macroscopic dissociation rate constant in collision of the $i$th molecule with $j$th heavy particle:

$$K_{D_{ij}} = \sqrt{(8R_A T/\pi\mu_{ij})}\sigma_{ij} \frac{N_A}{Z_i[T^{(v)}]} \frac{1}{(kT)^2} \exp\left(-\frac{T_{Di}}{T}\right) \cdot \Phi_{ij} \quad (26)$$

$$\Phi_{ij} = \frac{1}{2} \sum_{v=0}^{v_{i\,max}} \Phi_{vij} \quad (27)$$

$$\Phi_{vij} = (D_i - E_{v_i})(D_i - E_{v_i} + 2kT)\exp\left[-\left(\frac{1}{T_v} - \frac{1}{T}\right)\frac{E_{v_i}}{k}\right]$$

$$- \beta_{ij}\sqrt{D_i - E_{v_i}}\,\Big]$$

$$\beta_{ij} = \sqrt{\mu_{ij}/2N_A}/h\alpha_{ij} \quad (28)$$

$$Z_i[T^{(v)}] = \frac{1 - \exp[-T_{Di}/T^{(v)}]}{1 - \exp[-\theta_i/T^{(v)}]}$$

Thus, the physical constants $\theta_i$ and $D_i$, parameters of interaction with the collisional partner $\mu_{ij}$, $\sigma_{ij}$, and $\alpha_{ij}$, the translational and vibrational temperatures define the constant of dissociation unambiguously. An important feature of the dissociation rate model of Eq. (26) is a finiteness of the value of the constant at low temperatures. In nonequilibrium conditions, when $T^{(v)} < T$, the dissociation rate constant is less than that in the equilibrium case. However, the lowest value of $K_{D_{ij}}$ [when $T^{(v)} \to 0$] remains finite, its value corresponding to the dissociation from the ground vibrational state [the first term $\Phi_{0_{ij}}$ in sum (27)].

Expression (26) is too cumbersome for gasdynamic computations due to the necessity to sum $\Phi_{vij}$ over all the levels of the unharmonic oscillator for each $T$ and $T^{(v)}$. The dissociation rate model of Eq. (26) can, however, be simplified by using the harmonic oscillator model and separating a certain vibrational level $E_{v_i}^*$ whose effectiveness is equal to that of all the spectrum:

$$\Phi_{ij} = \tfrac{1}{2}(D_i - E_{v_i}^*)(D_i - E_{v_i}^*$$

$$+ 2kT)\exp[-\beta_{ij}\sqrt{D_i - E_{v_i}^*}]Z_i(T_m) \quad (29)$$

$T_m$ is defined by Eq. (13). Assuming that $E_{v_i}^* = 0$, we obtain

$$\Phi_{ij} = \tfrac{1}{2}D_i(D_i + 2kT)\exp(-\beta_{ij}\sqrt{D_i})Z_i(T_m) \quad (30)$$

Equation (30) is the simplest approximation of expression (27). It should be remarked that function $\Phi_{ij}(E_v)$ has a maximum at a certain $\bar{E}_v$: $\Phi_{ij}(\bar{E}_v) > \Phi_{ij}(0)$, and $\Phi_{ij} \to 0$ as $\bar{E}_v \to 0$ for every $i$th molecular species. Thus, approximation (30) of Eq. (27) is reasonable enough and corresponds to the assumption of equal dissociation probability from all the vibrational levels. At the same time expression (30) for $\Phi_{ij}$ can be improved. In Ref. 8 it has been proposed to obtain $\Phi_{ij}$ from the formula

$$\Phi_{ij} = \tfrac{1}{2}kT_{Di}\gamma_i(kT_{Di}\gamma_i + 2kT)\exp(-\beta_{ij}\sqrt{kT_{Di}\gamma_i}) \cdot Z_i(T_m) \quad (31)$$

where

$$\gamma_i = 1 - 0.8[\varepsilon_i(T_m)/R_A T_{Di}] \quad (32)$$

In other words, it is assumed[8] that $E_{v_i}^* = 0.8\varepsilon_i(T_m)/N_A$, where $\varepsilon_i$ is calculated by formula (8). It should be pointed out that the use of expression (28) to calculate $Z_i[T^{(v)}]$ yields quite accurate values of partition function because of relatively small values of $T^{(v)} < 1.5 \times 10^4$ K in hypersonic viscous shock layer under the conditions discussed. On the other hand, the use of expression (28) to calculate $Z_i(T_m)$, along with introduction of correction factor $\gamma_i$ in Eq. (31), is aimed at the formula-like approximation of Eq. (26) instead of summing up over all the levels of anharmonic oscillator. It has been shown in Ref. 8 that the difference between the ratios of vibrational nonequilibrium dissociation constants to thermal equilibrium ones $K_{D_{ij}}[T^{(v)}, T]/K_{D_{ij}}(T, T)$, obtained by means of approximate formula (31) and exact expression (27), lies within the scatter determined by the multiple $2.5^{\pm 1}$. It should be emphasized that the anharmonic effect in dissociation rate constants is not totally omitted in models (26) and (31). Expression (31) should be considered as a reasonable approximation of the original Eq. (27).

The main advantage of the described adiabatic model of Eq. (26) is in its unambiguity, which is based on the use of real physical quantities $\sigma_{ij}$ and $\alpha_{ij}$ instead of empirical parameters in expressions for dissociation rate constants. The quantities have a clear physical sense: $\sigma_{ij}$ is approximately equal to the gas-kinetic cross section and $\alpha_{ij}$ defines the repulsive part of the interaction potential. In the present study the values of $\sigma_{ij}$ and $\alpha_{ij}$ taken from Refs. 19 and 20, respectively, are used (see Table 1). Because of the low ionization under the conditions discussed, dissociation of the molecules $O_2$, $N_2$, and NO, due to their interactions with charged particles, is neglected. Recent comparisons of adiabatic dissociation constants with various experimental data under thermal equilibrium[8] have shown that the reaction rate model of Eq. (26) agrees well with the models of Blottner[21] and Park[16] at $T \lesssim$ 10,000 K (within the multiple of 3) and with the data of Baulch[22] (for $O_2$) and Kewley[23] (for $N_2$) at $T \geq$ 10,000 K (within the multiple of 5). In comparison, the uncertainty in the thermal equilibrium reaction rate constants suggested by various authors is much greater.
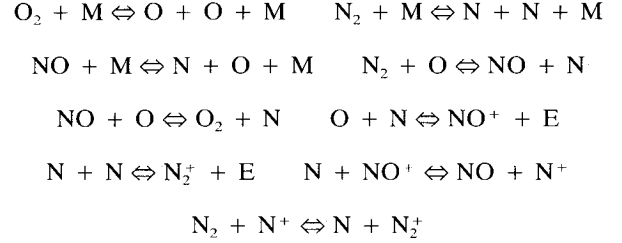
There are many models describing vibrational nonequilibrium. But all of these models either contain some undetermined empirical parameters or cannot be used (in gasdynamic codes) because of their complexity. The adiabatic dissociation rate model given by Eqs. (26) and (31) is simple, contains no empirical parameters, and accounts for both nonequilibrium vibrational excitation and equilibrium rotational excitation of the molecules. The model is the most physically adequate (among the models assuming Boltzmann distribution) because it permits the molecules to dissociate due to a violent rotation.[7,8] Nevertheless, there is an uncertainty in the model because of the scatter in experimental data on $\sigma_{ij}$ and $\alpha_{ij}$.

It is assumed that only rates of collisional dissociation reactions are determined by both $T$ and $T^{(v)}$, whereas those of all other reactions (recombination, ionization, and exchange reactions) are functions of the translational temperature $T$

**Table 1  Interaction parameters**

| Molecule | Partner | $\sigma_{ij}$, cm$^2$ | $\alpha_{ij}$, Å$^{-1}$ |
|---|---|---|---|
| $O_2$ | $O_2$ | $3.519 \times 10^{-15}$ | 2.85 |
|  | $N_2$ | $3.285 \times 10^{-15}$ | 3.02 |
|  | NO | $3.866 \times 10^{-15}$ | 3.78 |
|  | O | $2.807 \times 10^{-15}$ | 4.85 |
|  | N | $2.680 \times 10^{-15}$ | 4.13 |
| $N_2$ | $N_2$ | $3.058 \times 10^{-15}$ | 3.16 |
|  | NO | $3.620 \times 10^{-15}$ | 3.64 |
|  | O | $2.598 \times 10^{-15}$ | 5.12 |
|  | N | $2.476 \times 10^{-15}$ | 3.31 |
| NO | NO | $4.228 \times 10^{-15}$ | 3.26 |
|  | O | $3.117 \times 10^{-15}$ | 3.95 |
|  | N | $2.984 \times 10^{-15}$ | 3.72 |

only. The recombination rate constants are determined by the following expression:

$$K_{R_{ij}} = K_{D_{ij}}(T, T)/K_{c_i}(T, T) \qquad (33)$$

here, $K_{D_{ij}}$ are calculated by the formulas of Eqs. (26) and (31) and $K_{c_i}(T, T)$ are the equilibrium constants. The following reactions are considered:

$$O_2 + M \Leftrightarrow O + O + M \qquad N_2 + M \Leftrightarrow N + N + M$$

$$NO + M \Leftrightarrow N + O + M \qquad N_2 + O \Leftrightarrow NO + N$$

$$NO + O \Leftrightarrow O_2 + N \qquad O + N \Leftrightarrow NO^+ + E$$

$$N + N \Leftrightarrow N_2^+ + E \qquad N + NO^+ \Leftrightarrow NO + N^+$$

$$N_2 + N^+ \Leftrightarrow N + N_2^+$$

The exchange, ionization, and recharge reaction rate constants of Kang and Dunn (taken from Ref. 24) are used in the present study.

The transport properties necessary for the calculation of a viscous flow (the viscosity and thermal conductivity of the partially dissociated and ionized air mixture due to translational modes of the species) are determined using the approximate formulas suggested in Ref. 25. The formulas yield these coefficients with quite a good accuracy in a wide range of conditions. The contribution of rotational modes (and vibrational ones in the case of thermal equilibrium) to the heat conductivity of molecular species is accounted for by using the Eucken correction in the linear approximation.[26] It is known that the next approximations[27] of this correction differ negligibly from the linear one if the molecules are near spherical (as in the case of the air).

## IV.  Boundary Conditions

The Rankine–Hugoniot shock-slip relationships are used on the shock wave.[5] The following relationship between the $i$th species mass fraction in front of the shock and behind it is present:

$$c_{i\infty} = c_{is} - \frac{\cos(\beta_s)}{\rho_\infty V_\infty \sin(\beta)} J_{iy}\Big|_s \qquad (34)$$

The corresponding boundary condition for the $i$th molecular vibrational energy will be as follows:

$$c_i\varepsilon_i\Big|_\infty = c_i\varepsilon_i\Big|_s - \frac{\cos(\beta_s)}{\rho_\infty V_\infty \sin(\beta)}\left(\varepsilon_i J_{iy} - \mu \frac{c_i}{S_i}\frac{\partial\varepsilon_i}{\partial y}\right)\Big|_s \qquad (35)$$

The boundary condition for the average vibrational temperature $T^{(v)}$ is obtained by summing up Eqs. (35) over molecular species. Subscripts $\infty$ and $s$ in Eqs. (34) and (35) denote preshock and postshock conditions; $\beta_s = \beta - \alpha$; $\beta$ and $\alpha$ are the bow angles of the tangents to the shock and to the body with respect to axis of symmetry. In this article the flow conditions are considered where the shock wave is thin, and so, chemical reactions within the shock wave are not taken into account in condition (34), and the energy exchange between vibrational and active modes for the several collisions that occur in the shock wave is neglected in Eq. (35). It is known that the use of the shock-slip boundary conditions in VSL codes yields better agreement with DSMC rarefied flow solutions at high altitudes in comparison with no-shock-slip calculations.

On the body surface no-slip and no-flow conditions are used for momentum equation:

$$v_{1w} = 0, \qquad v_{2w} = 0 \qquad (36)$$

Subscript $w$ denotes the body surface conditions. Note that the wall-slip effects are negligible at high and moderate Reynolds numbers for the cold body surface. Radiation equilibrium of the surface is assumed for the energy conservation equation:

$$J_{qy}|_w = -\hat{\sigma}\hat{\varepsilon}T_w^4 \qquad (37)$$

$J_{qy}$ is the normal component of the heat transfer rate. In general, the energy flux is the sum of the heat transfer rate and dissipative term:

$$J_H = J_q - \hat{\tau}\cdot V$$

and if the conditions in Eq. (36) hold, $J_{Hy}|_w = J_{qy}|_w$. In Eq. (37) $\hat{\sigma} = 5.67 \times 10^{-8}$ W/m²K⁴ is a Stefan–Boltzmann's constant and $\hat{\varepsilon} = 0.8$ is the emissivity of the body surface. For the species mass conservation equations, the wall conditions can be written as follows:

$$J_{iy}|_w = -k_w\rho c_i|_w \qquad (38)$$

$k_w$ is an effective coefficient of catalytic activity of the surface. In the present work the extreme cases of the noncatalytic ($k_w = 0$) and the fully catalytic ($k_w = \infty$, i.e., $c_i|_w = 0$) walls are considered for the species O, N, and NO. The surface is supposed to be fully catalytic with respect to charged components. The diffusion fluxes of the elements $J_j^*$ onto a nondisintegrating surface are equal to zero. For the equation of vibrational relaxation the condition of thermal equilibrium on the body surface

$$T^{(v)}|_w = T_w \qquad (39)$$

and the condition of zero flux of vibrational energy onto the body

$$J_q^{\text{vib}} = \sum_{j=M} \frac{\varepsilon_j[T^{(v)}]}{m_j} J_j - \nabla T^{(v)}\mu \sum_{j=M} \varepsilon_j' \frac{c_j}{m_j S_j} = 0 \qquad (40)$$

have been considered. Here, the prime means differentiation with respect to $T^{(v)}$. Note that the expression for $J_q^{\text{vib}}$ directly follows from Eq. (16) and from the expression for thermal nonequilibrium heat flux, written in terms of $T$ and $\varepsilon_j$:

$$J_q = -\lambda^{\text{act}}\nabla T + \sum_{j=1}^{N} h_j J_j - \mu \sum_{j=M} \nabla\varepsilon_j \frac{c_j}{m_j S_j} \qquad (41)$$

In the case of the noncatalytic surface ($k_w = 0$), boundary conditions (39) and (40) are the extreme conditions for the equation of vibrational relaxation.[3,5] Note that when $k_w = 0$, condition (40) transforms to the more simple form

$$\frac{\partial T^{(v)}}{\partial y}\bigg|_w = 0 \qquad (42)$$

## V. Numerical Method

It is well known that the VSL equation set has elliptical properties. In order to overcome this difficulty the block-marching method of global iterations (GI)[9-12] is used in the present study. The method reduces the integration of the VSL system to several GI (i.e., marching procedures), the initial boundary-value problem solved along the body is well posed for each GI if there are no reversed flows.

The exact relationships to correctly calculate flow characteristics near the point of sphere-cone conjunction are given in Ref. 12. The governing equations are integrated using a second-order difference scheme along the body, while a fourth-order scheme is used normal to the body. The body is broken

down into blocks, and the method of global iterations is used both for the blunted part containing the sonic line (the first block) and for the conical part of the body (the other blocks) in the same way.

It takes the solution procedure, at the most, eight GIs to converge over the blunted part, and no more than three GIs at every block on the conical part of the body. The convergence criterion is max{$[\beta_s^{(n+1)} - \beta_s^{(n)}]/\beta_s^{(n)}$, $[P^{(n+1)} - P^{(n)}]/P^{(n)}$} < 0.01 for all grid points, where $n$ is the number of the global iteration.

At each step along the body the nonlinear MN VSL system is solved by using the Newton method. The fourth-order-difference scheme with a variable step along the normal coordinate enables one to obtain a reliable solution at large Reynolds numbers (up to $10^6$ or higher). No smoothing is needed for integrating the governing equations both in the streamwise and normal directions.

## VI. Results and Discussion

The main purposes of the present study are testing the developed algorithm for integration of the MN VSL equations and the investigation of nonequilibrium phenomena in the shock layer over a slender sphere-cone.

The calculations of the heat transfer rate to the body surface at the stagnation point, obtained with the model discussed, have been compared with those obtained by means of analytic Fay and Riddel's expression[28]:

$$J_{qw} = \rho_\infty V_\infty^3 \frac{0.763}{Pr^{0.6}} Re_\infty^{-0.5}\sqrt{\rho_e\mu_e u_e} \left(\frac{\rho_w\mu_w}{\rho_e\mu_e}\right)^{0.1} (H_e - H_w)A$$

$$A = \left[1 + (Le^{0.63} - 1)\frac{\sum_A h_i^0 C_{ie} - \sum_A h_i^0 C_{iw}}{H_e}\right] \qquad (43)$$

Here, indexes $w$ and $e$ correspond to the values on the body surface and at the edge of boundary layer, respectively (the edge of boundary layer was taken to be at a distance where the full enthalpy $H$ differs from $H_\infty$ by 5%); $\rho$ and $\mu$ are density and viscosity nondimensionalized by $\rho_\infty$ and $\mu_\infty$, respectively; $u = v_1/V_\infty \cos\alpha$ is the dimensionless tangential component of velocity; and $Le = Pr/Sc$, $Pr$ and $Sc$ are defined as the Prandtl and Schmidt numbers, respectively. The calculations have been carried out for partially dissociated air. The comparisons show that the difference between the values of $J_{qw}$ calculated by the MN VSL code and by formula (43) lies
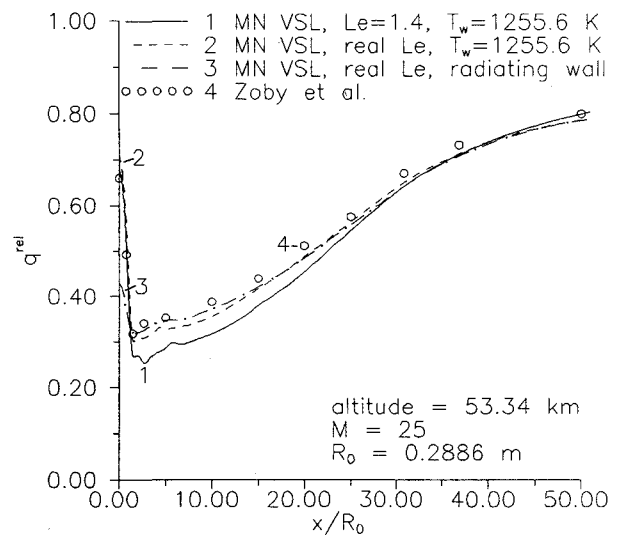


Fig. 1  Relative heating rate $H = 53.34$ km, $M_\infty = 25$.

within 6% over a wide range of $Re_\infty$ and $M_\infty$ numbers both for noncatalytic and fully catalytic surfaces. Note that Eq. (43) should be considered as that for rude assessments, especially when there is not full equilibrium in the "inviscid" flow.

Another comparison has been made with the calculations of Ref. 29. Relative values of the heat transfer rate

$$q^{\text{rel}} = J_{qw}|_{k_w=0}/J_{qw}|_{k_w=\infty} = J_{Hw}|_{k_w=0}/J_{Hw}|_{k_w=\infty}$$

are presented in that paper, $J_{qw}$ and $J_{Hw}$ are the normal components of the heat transfer rate and the energy flux to the body surface, respectively. The flow past a spherically blunted cone with a half-angle of 10 deg and a bluntness radius $R_0 = 0.2286$ m at a velocity $V_\infty = 8164$ m/s, altitude $H = 53.34$ km ($Re_\infty = 76,810$, $M_\infty = 25$), and $T_w = \text{const} = 1255.6$ K was chosen for the comparison. The calculations were carried out under the assumption of thermal equilibrium. Results of the comparison are presented in Fig. 1. Circles in this figure are data given in Fig. 3 of Ref. 29. Three types of calculations have been carried out: 1) under the assumption of binary diffusion with $Le = \text{const} = 1.4$ at $T_w = \text{const} = 1255.6$ K, as in Ref. 29 (solid line); 2) under the assumption of multicomponent diffusion with real binary diffusion coefficients at $T_w = \text{const} = 1255.6$ K (dashed line); and 3) those for radiatively equilibrium surface (39) (dash–dotted line). Multicomponent diffusion here means the use of Stefan–Maxwell relationships (8) instead of the binary diffusion model. The "real" binary diffusion coefficients are calculated by the formula:

$$D_{ij} = 8.256 \times 10^{-7} \left( T^3 \frac{m_i + m_j}{2m_i m_j} \right)^{1/2} \frac{1}{P(\text{atm})Q_{ij}^{11}} \text{ m}^2/\text{s}$$

(44)

$m_i$ are measured in atomic units. Interaction integrals $Q_{ij}^{11}$ and $Q_{ij}^{22}$ ($\mathring{A}^2$), the latter being necessary for the calculation of viscosity and thermal conductivity, are taken from Ref. 20. At the stagnation point the value of $q^{\text{rel}}$ obtained using MN VSL code with $Le = 1.4$ coincides with that represented in Ref. 29 remarkably well. But downstream a discrepancy occurs: up to 33% in the region where $q^{\text{rel}}$ is minimum, and less than 4% at $x/R_0 \geq 30$, $x$ being a distance measured from the stagnation point along the body surface and $R_0$ being the bluntness radius. The disagreement may be due to the smoothing used in Ref. 29. Note that in the case of a radiatively equilibrium wall, $T_w|_{k_w=0} = 2774$ K and $T_w|_{k_w=\infty} = 3424$ K at the stagnation point. The value of $q^{\text{rel}}$ in this case is 40% smaller than the corresponding value obtained with $T_w = \text{const} = 1255.6$ K with the real diffusion model used in both cases.

Represent explicitly $J_{qw}$ values for radiatively equilibrium wall (see Table 2). From these data one can see that at the stagnation point:

1) The agreement of $J_{qw}$ values with those obtained from expression (43) is satisfactory.

2) Real Lewis number may differ significantly from 1.4 throughout the shock layer.

3) The combined effect of multicomponent diffusion and real diffusion coefficients on the heat transfer rate may reach 17% for the noncatalytic wall and 23% for the fully catalytic wall at the stagnation point. On the cone the difference of the "multicomponent" heat flux values from "binary" ones does not exceed 23%.

Figure 2 shows heat transfer rate, shock standoff distance, and pressure along the body for the previously mentioned conditions under the assumption of multicomponent diffusion with binary diffusion coefficients calculated via pressure, temperature, and interaction integrals. In the figure the body surface is assumed to be in the radiative equilibrium, i.e.,

Table 2  Heat flux values at the stagnation point; comparison with Fay and Riddel's formula (43)

| | $J_{qw}$, W/m$^2$, MN VSL | $J_{qw}$, W/m$^2$, Fay–Riddel | |
|---|---|---|---|
| $k_w = 0$, $Le = 1.4$ | $5.69 \times 10^6$ | $5.50 \times 10^6$ | |
| $k_w = \infty$, $Le = 1.4$ | $8.38 \times 10^6$ | $7.87 \times 10^6$ | |
| $k_w = 0$ | $1.14 \geq Le \geq 0.78$ $4.85 \times 10^6$ | $Le = 1$ $4.85 \times 10^6$ | $Le = 1.4$ $5.39 \times 10^6$ |
| $k_w = \infty$ | $1.45 \geq Le \geq 0.78$ $6.83 \times 10^6$ | $Le = 1$ $6.48 \times 10^6$ | $Le = 1.4$ $7.51 \times 10^6$ |

$H = 53.34$ km, $V_\infty = 8164$ m/s ($Re_\infty = 76,810$, $M_\infty = 25$), $T_w = 1255.6$ K, $T^{(v)} = T$.
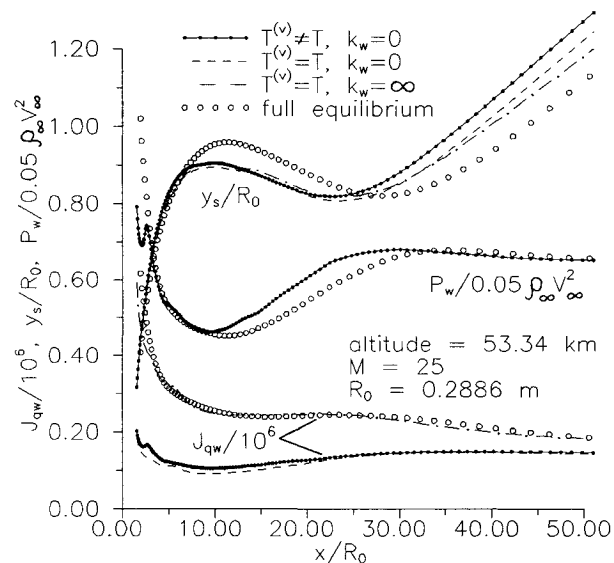


Fig. 2  Absolute heating rate, shock standoff distance, and wall pressure, $H = 53.34$ km, $M_\infty = 25$.

boundary condition (37) is used for energy equation. In the figure the heat transfer rate to the body surface $J_{qw}$ (W/m$^2$), shock standoff distance $y_s/R_0$, and the wall pressure $P_w$ nondimensionalized by the value $\rho_\infty V_\infty^2$ are plotted vs $x/R_0$. It should be emphasized that all the calculations presented in this article have been carried out for the long sphere-cone (up to $x/R_0 = 300$). But the main transformations of the flow occur within the region $0 < x/R_0 < 50$. Therefore, in order to make this article more informative, attention is focused on this region for the results presented in all the figures. From Fig. 2 one can see that the catalytic activity changes the shock standoff distance within 4.5%. The fully equilibrium calculations were carried out with use of the algorithm developed in Refs. 9–12 for the simulation of chemical (and thermal) equilibrium and chemical (and thermal) frozen flows past slender spherically blunted cones. The calculations for thermal and chemical nonequilibrium were carried out with use of boundary conditions (39) and (42) for the noncatalytic wall only. It has been shown in Ref. 5 that the influence of thermal nonequilibrium on the heat transfer rate onto the fully catalytic wall is small.

The fully nonequilibrium calculations are presented by solid lines connecting closed circles. The points correspond to positions of the normal grid lines (rays) in the axial direction. The grid has been used for the most of calculations discussed. The grid has been considered twice as frequently for separate calculations to check the grid convergence of solution, especially in nonmonotoneous regions. The fully equilibrium calculations (open circles) have been obtained with use of a more coarse grid. The implemented grids are automatically extended along the body length.

Table 3 Heat flux and shock standoff distance values at the stagnation point. Comparison of thermodynamic models, the wall being under radiation equilibrium

| | $J_{qw}$, W/m$^2$ | $y_s/R_0$ |
|---|---|---|
| $k_w = 0$, $T^{(v)}\mid_w = T_w$ | $3.17 \times 10^6$ | $6.05 \times 10^{-2}$ |
| $k_w = 0$, $\dfrac{\partial T^{(v)}}{\partial y}\bigg\mid_w = 0$ | $2.78 \times 10^6$ | $6.10 \times 10^{-2}$ |
| $k_w = 0$, $T^{(v)} = T$ | $2.69 \times 10^6$ | $5.73 \times 10^{-2}$ |
| $k_w = \infty$, $T^{(v)} = T$ | $6.25 \times 10^6$ | $5.70 \times 10^{-2}$ |
| Full equilibrium | $6.45 \times 10^6$ | $4.81 \times 10^{-2}$ |

$H = 53.34$ km, $V_\infty = 8164$ m/s ($Re_\infty = 76,810$, $M_\infty = 25$).
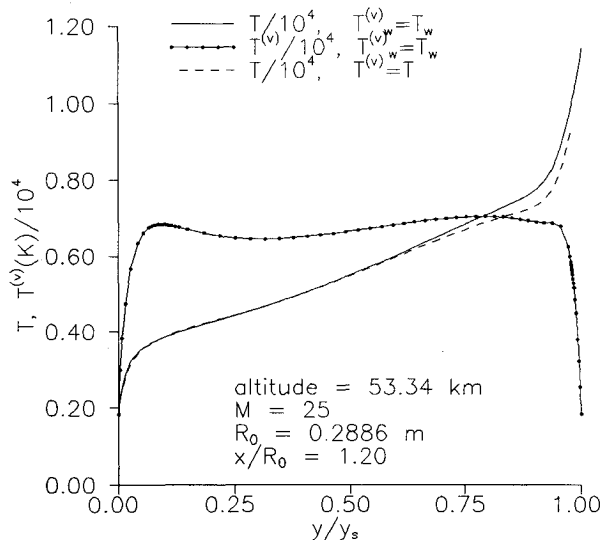


Fig. 3 Temperatures, $x/R_0 = 1.20$.
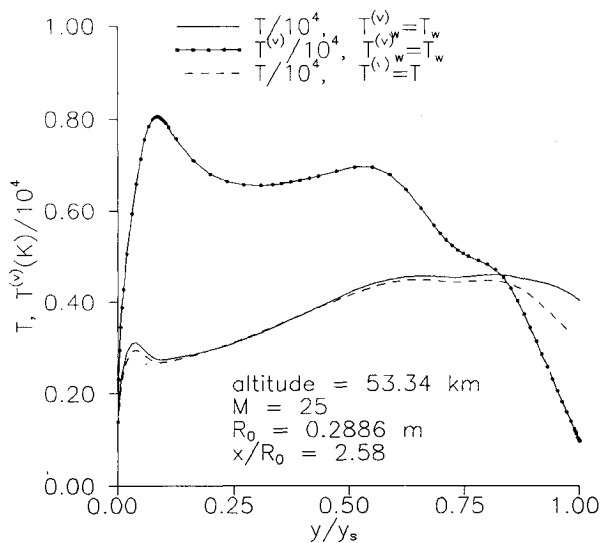


Fig. 4 Temperatures, $x/R_0 = 2.58$.

The heat flux and shock standoff distance at the stagnation point are given in Table 3. From the table we see that thermal nonequilibrium value of the heat transfer rate at the stagnation point differs from thermal equilibrium value by 18% if the boundary condition (39) is used. In the case of zero flux of vibrational energy to the noncatalytic wall [boundary condition (40) or (42)], the thermal nonequilibrium value of the heating rate differs from the thermal equilibrium one by 3.4%. The difference between thermal nonequilibrium and equilibrium values of the shock standoff distance is within 6.5%, and the chemical nonequilibrium value of the shock standoff

distance under thermal equilibrium differs from the fully equilibrium value by 15.5% for $k_w = \infty$. The difference between fully nonequilibrium (when both thermal and chemical nonequilibrium are assumed) and fully equilibrium values of pressure is about 1.5%.

As noted by others in the past, there is a similarity between the behavior of the heat transfer rate and of the pressure along the body. It should be pointed out that the surface pressure distribution in turn is similar to that of the quantity $dy_s/dx$ at the conical part of the body (not shown in the figure). The quantity $dy_s/dx$ is not monotone near the point with minimum pressure. It cannot be a numerical error because different grids, block sizes, and block intersections have been considered. It is obvious that the effect will not be displayed if any artificial numerical smoothing is used in the streamwise direction. Note once more that the immediate sphere-cone conjunction with curvature discontinuity is assumed in the present study.

Figures 3–5 show the profiles of translational and vibrational temperatures across the shock layer plotted vs $y/y_s$, here $y_s$ is the shock standoff distance for the case of thermal and chemical nonequilibrium. In these figures, the surface is assumed to be noncatalytic and the boundary condition (39) is used for the equation of vibrational relaxation. Figure 3 corresponds to the station on the spherical part of the body before the sphere-cone conjunction, Fig. 4 corresponds to the position of nonmonotonicity in $P_w$ and $J_{qw}$ values, and Fig. 5 corresponds to the station near the local minimum of $y_s$ values. These sections have been chosen to demonstrate the complexity of the flow thermodynamics that is due to the chemical reactions, energy-exchange processes, and heat and mass transfer. Profiles of $T$ and $T^{(v)}$ at other $x/R_0$ values can be found in Ref. 30.

Profiles of $T^{(v)}$ (solid lines connecting black points) demonstrate the grid in a normal direction. About 70 points have been used across the layer. The grid is condensed in the regions with large gradients and second derivatives of $T$ and $T^{(v)}$. Various criteria for condensing the grid have been considered in order to validate the solutions obtained.

Analyzing Figs. 3–5, one can see that vibrational relaxation is a very inertial process, i.e., when the flow cools moving along the body, the vibrational temperature lags from translational one, remaining similar to the upstream $T^{(v)}$ profiles. In the figures the maximum values of $T^{(v)}$ are higher than those of $T$. A peak of vibrational temperature near the wall is due to the recombination in the vicinity of the relatively cold body surface. The process contributes a large energy into vibrational modes, according to the CVDV model imple-
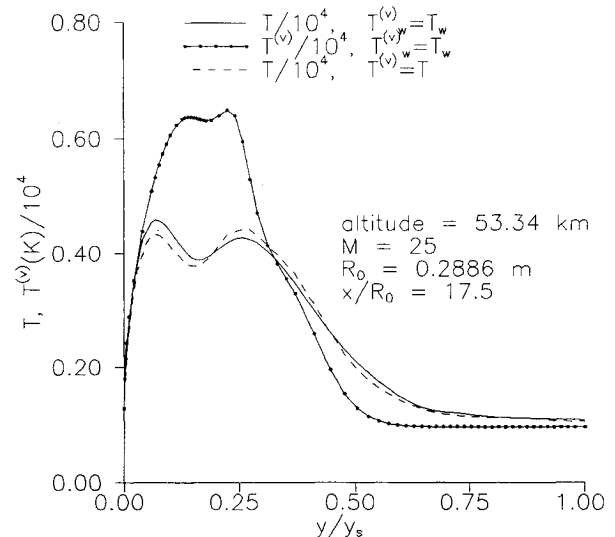


Fig. 5 Temperatures, $x/R_0 = 17.5$.

**Table 4   Heat flux and shock standoff distance values at the stagnation point; comparison of thermodynamic models, the wall being under radiation equilibrium**

|  |  | $J_{qw}$, W/m$^2$ | $y_s/R_0$ |
| --- | --- | --- | --- |
| $H = 53.34$ km, $V_\infty = 4,898$ m/s | $T^{(v)}\vert_w = T_w$ | $6.39 \times 10^5$ | $8.52 \times 10^{-2}$ |
| ($Re_\infty = 46,080$, $M_\infty = 15$) | $T^{(v)} = T$ | $6.10 \times 10^5$ | $8.12 \times 10^{-2}$ |
| $H = 68.58$ km, $V_\infty = 7,492$ m/s | $T^{(v)}\vert_w = T_w$ | $7.76 \times 10^5$ | $7.95 \times 10^{-2}$ |
| ($Re_\infty = 11,850$, $M_\infty = 25$) | $T^{(v)} = T$ | $7.06 \times 10^5$ | $7.19 \times 10^{-2}$ |
| $H = 53.34$ km, $V_\infty = 2,500$ m/s | $T^{(v)}\vert_w = T_w$ | $1.05 \times 10^5$ | $1.37 \times 10^{-1}$ |
| ($Re_\infty = 23,520$, $M_\infty = 7.86$) | $T^{(v)} = T$ | $1.05 \times 10^5$ | $1.21 \times 10^{-1}$ |

$k_w = 0$.

**Table 5   Maximum values of species concentrations; comparison of thermodynamic models**

|  |  | O, cm$^{-3}$ | N, cm$^{-3}$ | NO, cm$^{-3}$ | E, cm$^{-3}$ |
| --- | --- | --- | --- | --- | --- |
| $H = 53.34$ km, $M_\infty = 25$ | $T^{(v)}\vert_w = T_w$ | $2.95 \times 10^{17}$ | $4.22 \times 10^{17}$ | $1.31 \times 10^{16}$ | $6.36 \times 10^{14}$ |
|  | $T^{(v)} = T$ | $2.99 \times 10^{17}$ | $5.25 \times 10^{17}$ | $9.22 \times 10^{15}$ | $5.91 \times 10^{14}$ |
| $H = 68.58$ km, $M_\infty = 25$ | $T^{(v)}\vert_w = T_w$ | $5.12 \times 10^{16}$ | $8.34 \times 10^{16}$ | $1.96 \times 10^{15}$ | $5.61 \times 10^{13}$ |
|  | $T^{(v)} = T$ | $5.24 \times 10^{16}$ | $9.03 \times 10^{16}$ | $1.42 \times 10^{15}$ | $5.15 \times 10^{13}$ |
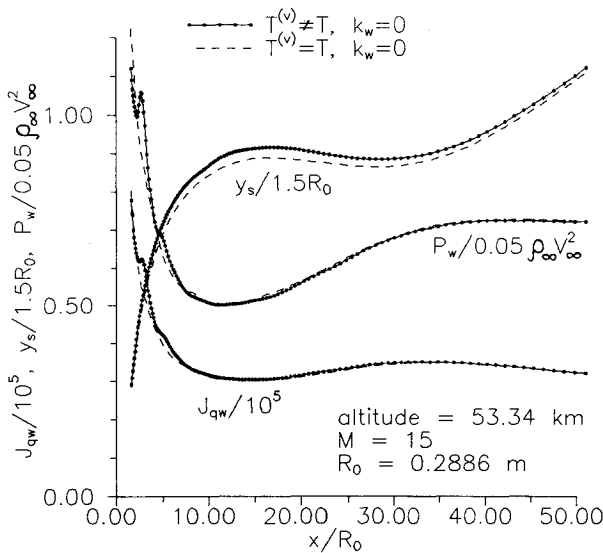


Fig. 6   Absolute heating rate, shock standoff distance, and wall pressure, $H = 53.34$ km, $M_\infty = 15$.



Fig. 7   Absolute heating rate, shock standoff distance, and wall pressure, $H = 68.58$ km, $M_\infty = 25$.

mented in the present study. Note that two sublayers are gradually formed in the flow along the cone: "cold" and "hot." In the cold sublayer the flow remains thermally frozen with $T^{(v)} < T$. In the hot sublayer $V$-$T$ process and dissociation/recombination affect the vibrational energy of the mixture. But there is no thermal equilibrium all over the shock layer because of the previously mentioned lagging of vibrational temperature.

Figure 6 gives the values of the heat transfer rate to the body, shock standoff distance, and pressure along the non-catalytic radiatively equilibrium surface of the same body at $H = 53.34$ km, $V_\infty = 4898$ m/s ($Re_\infty = 46,080$, $M_\infty = 15$). Figure 7 shows the same quantities at $H = 68.58$ km, $V_\infty = 7492$ m/s ($Re_\infty = 11,850$, $M_\infty = 25$). For the equation of vibrational relaxation thermal equilibrium of the surface is assumed. The corresponding stagnation-point data are given in Table 4. The last conditions in the table have been chosen to assess the pure effect of thermal nonequilibrium on the shock standoff distance over the bluntness. Actually, there are no chemical reactions at these conditions, and the 13% difference in $y_s/R_0$ is solely due to the vibrational energy that noticeably differs in the cases of thermal equilibrium and nonequilibrium. Thus, at the stagnation point the effect of thermal nonequilibrium on the heat flux is no more than 10% and on the shock standoff distance it is no more than 13% for these three flows.

On the conic part of the body, the thermal nonequilibrium values of the heat transfer rate differ from the corresponding thermal equilibrium values by no more than 20% for the conditions of Figs. 2, 6, and 7, and the influence of thermal nonequilibrium on the shock standoff distance is within 6%.

Finally, the maximum values of the concentrations of atomic oxygen, atomic nitrogen, nitrogen oxide, and electrons across the shock layer at the stagnation point are provided (see Table 5). Analyzing these figures and the results of downstream calculations, we can say that in the region, encompassing the stagnation point and the sphere-cone conjunction, the effect of thermal nonequilibrium on the concentration of atomic oxygen is within 5%, on atomic nitrogen it is within 20%, on the concentration of nitrogen oxide it is within 42%, and on that of electrons it is within 9% at the conditions discussed. Downstream the fractions of these species go down, and the effect may be greater. Note that in the stagnation region thermal nonequilibrium concentrations of atomic oxygen and nitrogen are less than corresponding thermal equilibrium values, but those of nitrogen oxide and electrons are greater.

## VII.   Conclusions

The comparison with the results of Ref. 29 has shown that at the stagnation point the value of the heating rate for the noncatalytic surface related to that for the fully catalytic one agree with the corresponding value of Ref. 29 within 3%. But downstream a discrepancy occurs: up to 33% in the region

where the relative heating rate is minimum, and less than 4% at $x/R_0 \geq 30$. The discrepancy may be due to the smoothing used in Ref. 29.

The code has been compared also with the previously developed code for the calculation of perfect-gas flows and fully equilibrium ones.[9-12] In both cases the MN VSL code yields a good agreement of calculations with those obtained by the algorithm.[9-12]

The effect of thermal nonequilibrium on pressure is negligible. The influence of thermal nonequilibrium on the heat transfer rate is within 20% and on the shock standoff distance it is no more than 13%.

There is a nonmonotonicity of the wall pressure and the heat flux to the body not far from the stagnation point. The effect occurs at certain regimes when the flow is assumed to be thermal equilibrium and chemical nonequilibrium and is strengthened under both thermal and chemical nonequilibrium (see Figs. 2, 6, and 7). It is not a numerical effect. The behavior of $P_w$ and $J_{qw}$ is connected with corresponding nonmonotonicity of the derivative $dy_s/dx$ in the region where overexpansion takes place.

The extreme boundary conditions (39) and (40) have been considered for the equation of vibrational relaxation. The difference between the corresponding values of the heat flux onto the noncatalytic wall is within 15%.

The real Lewis numbers in multicomponent chemical nonequilibrium gas mixture substantially differ from the value of 1.4. And the combined effect of the real binary diffusion coefficients and multicomponent diffusion on the heat transfer rate may be as large as 23%.

In comparison with fully equilibrium calculations, the effect of chemical nonequilibrium on pressure is negligible all over the body. In the case of chemical nonequilibrium the heat transfer rate to the fully catalytic surface is close to that onto a fully equilibrium one. There is a region not far from the stagnation point where the fully equilibrium shock standoff distance turns out to be greater than the nonequilibrium one (see Fig. 2). It can be due to a more intensive recombination near the spherical bluntness in the case of chemical equilibrium because in this case species concentrations depend more rigidly on the pressure and the mixture static enthalpy along the body than in the case of nonequilibrium. Since the equilibrium recombination is more intensive, there is a more intensive energy release in the stagnation region, which, in turn, leads to a higher temperature and lower density. Therefore, the equilibrium shock standoff distance becomes greater than the nonequilibrium one in this region. At large distances from the stagnation point the fully equilibrium shock standoff distance is 5% less than chemical nonequilibrium and thermal equilibrium one, and the fully (both chemical and thermal) nonequilibrium shock standoff distance is 6% greater than chemical nonequilibrium and thermal equilibrium one.

Calculations have shown that at $x/R_0 \geq 30$ the flow becomes qualitatively invariant with a cold region behind the shock and a hot sublayer near the wall (see also Ref. 30). The quantitative changes consist only in a decrease of the relative thickness of the hot sublayer where $T$ and $T^{(v)}$ across the shock layer are maximum. In the cold sublayer over conic part of the body there is no equilibrium between the active and vibrational modes. It is caused by very large values of relaxation time $\tau_1$ at low temperatures and pressures. Therefore, the flow remains frozen both chemically and thermally in this part of the flow.

The results of the present study indicate that thermal nonequilibrium has a relatively small effect on "macroscopic" flow characteristics and may noticeably affect some "fine" parameters, such as concentrations of certain species. Therefore, the further development of the modeling nonequilibrium processes in high-enthalpy gas mixtures is necessary to create reliable codes for simulation of hypersonic flows over a wide range of freestream conditions.

## References

[1]Davis, R. T., and Flugge-Lotz, I., "Second-Order Boundary-Layer Effects in Hypersonic Flow past Axisymmetric Blunt Bodies," *Journal of Fluid Mechanics*, Vol. 20, No. 4, 1964, pp. 593–623.

[2]Davis, R. T., "Numerical Solution of the Hypersonic Viscous Shock-Layer Equations," *AIAA Journal*, Vol. 8, No. 5, 1970, pp. 843–851.

[3]Tirsky, G. A., "Up-to-Date Gasdynamic Models of Hypersonic Aerodynamics and Heat Transfer with Real Gas Properties," *Annual Review Fluid Mechanics*, Vol. 25, 1993, pp. 151–181.

[4]Cheng, H. K., "Hypersonic Shock-Layer Theory of the Stagnation Region at Low Reynolds Number," *Proceedings of the Institute of Heat Transfer and Fluid Mechanics*, Stanford Univ. Press, Stanford, CA, 1961, pp. 161–175.

[5]Zhluktov, S. V., and Tirskiy, G. A., "An Effect of Vibration-Dissociation Coupling on the Heat Transfer and Aerodynamic Resistance in Hypersonic Flows past Blunt Bodies," *Izvestija Akademii Nauk USSR. Mekhanika Zhidkosti i Gaza*, No. 3, 1990, pp. 141–151 (in Russian).

[6]Marrone, P. V., and Treanor, C. E., "Chemical Relaxation with Preferential Dissociation from Excited Vibrational Levels," *Physics of Fluids*, Vol. 6, No. 9, 1963, pp. 1215–1222.

[7]Smekhov, G. D., and Zhluktov, S. V., "The Rate Constants of Adiabatic Dissociation of Diatomic Molecules," *Khimicheskaya Fizika*, Vol. 11, No. 5, 1992, pp. 1171–1179 (in Russian).

[8]Zhluktov, S. V., Smekhov, G. D., and Tirskiy, G. A., "Rotation-Vibration-Dissociation Coupling in Multicomponent Nonequilibrium Viscous Shock Layer," *Izvestija Rossiyskoy Akademii Nauk. Mekhanika Zhidkosti i Gaza*, No. 6, 1994, pp. 166–179 (in Russian).

[9]Utyuzhnikov, S. V., "A Numerical Solution of the Full Viscous Shock Layer Equations of Hypersonic Flows past Blunt Bodies," *Chislennye Metody Mekhaniki Sploshnykh Sred*, Vol. 17, No. 6, Novosibirsk, Russia, 1986, pp. 125–131 (in Russian).

[10]Vasilievskiy, S. A., Utyuzhnikov, S. V., and Tirskiy, G. A., "Numerical Method for Solution of Viscous Shock Layer Equations," *Jurnal Vychislitelnoi Matematiki i Matematicheskoi Fiziki*, Vol. 27, No. 5, 1987, pp. 741–750 (in Russian).

[11]Andriatis, A. V., and Utyuzhnikov, S. V., "Numerical Simulation of Viscous and Heat-Conducting Gas Flows past Slender Bodies with Account of Actual Physical Properties of the Medium and Three-Dimensional Radiation Transfer," *Modelirovanie v Mekhanike*, Vol. 2(19), No. 1, Novosibirsk, Russia, 1988, pp. 3–10 (in Russian).

[12]Tirskiy, G. A., Utyuzhnikov, S. V., and Yamaleev, N. K., "Efficient Numerical Method for Simulation of Supersonic Flow past Blunted Body at Small Angle of Attack," *Computers and Fluids Journal*, Vol. 23, No. 1, 1994, pp. 103–114.

[13]Scherbak, V. G., "On the Influence of the Multi Component Diffusion and Baro-Diffusion on the Element Composition for Hypersonic Flows," *Injenerno-Fizicheskiy Jurnal*, Vol. 59, No. 4, 1990, pp. 673, 674 (in Russian).

[14]Apshtein, E. E., Pilyugin, N. N., and Tirskiy, G. A., "Radiation Transfer for Blunt Bodies Entering the Atmosphere of a Planet with Super-Orbital Velocities," *Itogi nauki i tekhniki. Mekhanika Zhidkosti i Gaza*, Vol. 23, VINITI, Moscow, 1989, pp. 116–236 (in Russian).

[15]Tirskiy, G. A., "Hemiphenomenological Deriving Equations for Mixtures of Polyatomic Gases with Exited Quantum States," *Mekhanika. Sovremennye Problemy*, edited by G. G. Chernyi, Inst. of Mechanics at Moscow Univ., Moscow, 1987, pp. 79–86 (in Russian).

[16]Millikan, R. C., and White, D. R., "Systematics of Vibrational Relaxation," *Journal of Chemical Physics*, Vol. 39, No. 12, 1963, pp. 3209–3213.

[17]Park, C., "Problem of Rate Chemistry in the Flight Regimes of Aeroassisted Orbital Transfer Vehicles," AIAA Paper 84-1730, 1984.

[18]Park, C., "Assessment of Two-Temperature Kinetic Model for Ionizing Air," AIAA Paper 87-1574, 1987.

[19]*Thermodynamic and Thermophysic Properties of Combustion Products*, edited by V. P. Glushko, Vols. 1–10, VINITI, Moscow, 1973 (in Russian).

[20]Gordeev, O. A., Kalinin, A. P., Komov, A. L., Lusternik, V. E., Samuilov, E. V., Sokolova, I. A., and Fokin, L. R., "Interaction Potentials, Elastic Cross-Sections, and Collision Integrals for the Air

Species up to 20000 K (Methods of Estimation, Recommended Data)," *Reviews on Thermophysic Properties of Species*, No. 5(55), Inst. of High Temperatures, USSR Academy of Sciences, Moscow, 1985 (in Russian).

[21]Blottner, F. G., "Viscous Shock Layer at the Stagnation Point with Nonequilibrium Air Chemistry," *AIAA Journal*, Vol. 7, No. 12, 1969, pp. 2281–2288.

[22]Baulch, D. L., Drysdale, D. D., Duxbury, J., and Grant, S. L., "Evaluated Kinetic Data for High Temperature Reactions," Vol. 3, Butterworths, London, 1976.

[23]Kewley, D. J., and Hornung, H. G., "Free-Piston Shock-Tube Study of Nitrogen Dissociation," *Chemical Physics Letters*, Vol. 25, No. 4, 1974, pp. 531–536.

[24]Swaminathan, S., Song, D. J., and Lewis, C. H., "Effects of Slip and Chemical Reaction Models on Three-Dimensional Nonequilibrium Viscous Shock-Layer Flows," *Journal of Spacecraft and Rockets*, Nov.–Dec. 1984, pp. 521–527.

[25]Andriatis, A. V., Zhluktov, S. V., and Sokolova, I. A., "Trans-

port Coefficients of Nonequilibrium Air Mixture," *Matematicheskoe Modelirovanie*, Vol. 4, No. 1, 1992, pp. 44–65 (in Russian).

[26]Girshfelder, G. U., "Heat Conductivity in Polyatomic and Electronically Excited Gases," *Journal of Chemical Physics*, Vol. 26, No. 2, 1957, pp. 282–285.

[27]Monchick, L., Pereira, A. N. G., and Mason, E. A., "Heat Conductivity of Polyatomic and Polar Gas Mixtures," *Journal of Chemical Physics*, Vol. 42, No. 9, 1965, pp. 3241–3256.

[28]Dorrance, W. H., *Viscous Hypersonic Flow. Theory of Reacting and Hypersonic Boundary Layers*, McGraw–Hill, New York, 1962.

[29]Zoby, E. V., Lee, K. P., Gupta, R. N., Tomson, R. A., and Simmonds, A. L., "Viscous Shock Layer Analysis of Nonequilibrium Flows past Thin Slender Bodies," *Journal of Spacecraft and Rockets*, Vol. 26, No. 4, 1989, pp. 221–228.

[30]Zhluktov, S. V., Tirskii, G. A., and Utyuzhnikov, S. V., "Thermally Non-Equilibrium Viscous Shock Layer Past Slender Blunted Cones," *Prikladnaya Matematika i Mekhanika*, Vol. 58, No. 3, 1994, pp. 493–505.